ACS APPLIED MATERIALS & INTERFACES

Research Article

www.acsami.org

Composite Manganese Oxide Percolating Networks As a Suspension Electrode for an Asymmetric Flow Capacitor

Kelsey B. Hatzell,[†] Lei Fan,[†] Majid Beidaghi,[†] Muhammad Boota,[†] Ekaterina Pomerantseva,[†,§] Emin C. Kumbur,*[,‡] and Yury Gogotsi*[,†]

[†]A.J. Drexel Nanomaterials Institute, Department of Material Science and Engineering, Drexel University, 3141 Chestnut Street, Philadelphia, Pennsylvania 19104, United States

[‡]Electrochemical Energy Systems Laboratory, Department of Mechanical Engineering and Mechanics, Drexel University, 3141 Chestnut Street, Philadelphia, Pennsylvania 19104, United States

[§]Materials Electrochemistry Group, Department of Material Science and Engineering, Drexel University, 3141 Chestnut Street,Philadelphia, Pennsylvania 19104, United States

Supporting Information

ABSTRACT: In this study, we examine the use of a percolating network of metal oxide (MnO_2) as the active material in a suspension electrode as a way to increase the capacitance and energy density of an electrochemical flow capacitor. Amorphous manganese oxide was synthesized via a low-temperature hydrothermal approach and combined with carbon black to form composite flowable electrodes of different compositions. All suspension electrodes were tested in static configurations and consisted of an active solid material (MnO_2 or activated carbon) immersed in aqueous neutral electrolyte (1 M Na_2SO_4). Increasing concentrations of carbon black led to better rate performance but at the cost of capacitance and viscosity. Furthermore, it was shown that an expanded voltage window of 1.6 V could be achieved when combining a composite MnO_2-carbon black (cathode) and an activated carbon suspension (anode) in a charge balanced asymmetric device. The expansion of the voltage window led to a significant increase in the energy density to ~11 Wh kg^{-1} at a power density of ~50 W kg^{-1}. These values are ~3.5 times and ~2 times better than a symmetric suspension electrode based on activated carbon.

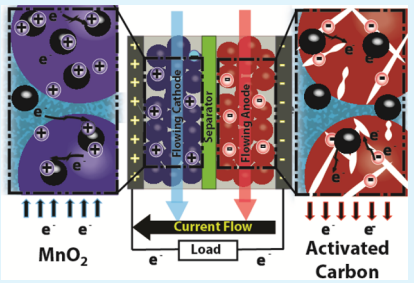

KEYWORDS: *asymmetric supercapacitor, electrochemical flow capacitor, flowable electrode, manganese oxide, percolating networks, suspension electrode*

1. INTRODUCTION

For the practical implementation of energy storage at the grid level, novel technologies based on cheap, environmentally friendly, and abundant materials are needed.[1,2] In the past couple of years, there has been a renaissance of new electrochemical energy storage technologies that have evolved to address the challenge of integrating energy storage into the electricity infrastructure.[1,3−6] Many of these systems adopt several of the key benefits derived from flow battery systems, namely, the ability to obtain both scalable energy and power densities at a lower cost.[7,8] Among, these new systems, a new type of energy storage based on flowable suspension-type electrodes has emerged as a possible method for achieving high charge capacity.[9−12]

Suspension electrodes or flowable electrodes are slurries where the majority component is the electrolyte. Flowable electrodes enable the scale-up of electrochemical energy storage systems traditionally used in small-scale portable electronics in order to address a wider range of applications. Furthermore, suspension electrodes are electrically conducting in nature in contrast with traditional flow-batteries which utilize an electronically insulating redox-electrolyte for reversible charge storage. These suspensions are formed by combining nano- or microsized active materials in an electrolytic media in order to facilitate charge storage and conductivity through percolating networks.[13] The connectivity exhibited between active particles allows for continuous and scalable charge storage (Figure 1b).

Electrochemical capacitor (electrochemical flow capacitor[11]) and battery (semi-solid lithium battery[10,14]) systems utilize this concept for grid level energy storage. In both cases, the electrolyte aids in the transportation of the active materials such that the charge can be stored in a scalable manner. The former relies on charge storage in an electric double layer, whereas the latter relies on chemical reactions for charge storage. Most recently, the idea of flowing capacitive suspension electrode (CSEs) has also been extended to desalination, as a means for scaling up capacitive deionization systems.[15−17]

For high-rate grid applications, such as frequency regulation, where fluctuations of MW/min need to be accommodated, rapid charging/discharging is desirable. Thus, suspension

Received: March 19, 2014
Accepted: April 23, 2014
Published: April 23, 2014

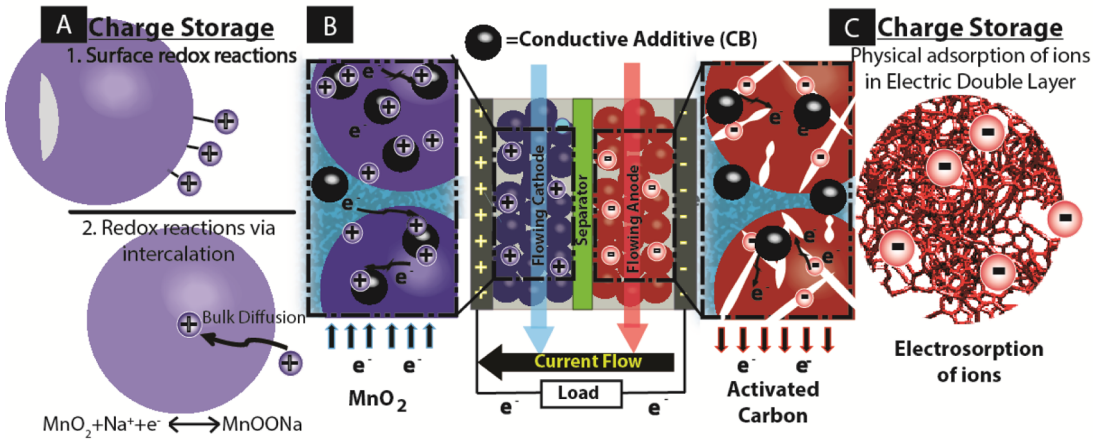

Figure 1. (A) Two charge storage mechanisms utilized in MnO_2 suspension electrodes, (B) a schematic of an asymmetric flowable electrode system based on manganese oxide and activated carbon suspensions, and (C) the electric double layer charge storage in the porous carbon anode.

electrodes based on capacitive electrode materials (electrostatic charge storage) are ideal candidates for addressing this need. Nevertheless, while electrochemical capacitors are known for their high power capabilities, they often exhibit lower energy densities when compared with battery systems.[18] To improve this quality, researchers have examined redox-active electrolytes[12,19,20] and transition metal oxides as a way to enhance the capacitance via the addition of fast redox reactions (pseudocapacitance).[21−24] Manganese oxide (MnO_2) has been shown to be one of the most promising and pragmatic materials that has potential for large-scale applications because it is low cost, environmentally friendly, and abundant[25−28]- (Figure 1a). Another benefit of MnO_2 based electrodes, is their ability to work in neutral aqueous electrolytes, which is ideal for large scale systems.[29] Although supercapacitors based on porous carbon store charge at the surface through the formation of an electric double layer (Figure 1c), manganese oxide undergoes redox reactions, either through chemisorption at the surface, or through intercalation of a charge carrier cation into the bulk (Figure 1a).[30] The benefit of the later is that charge storage capacity is not limited by the surface area, and thus high capacitance can be achieved.

In aqueous-electrolyte systems, the voltage window is typically limited to <1.23 V because of water decomposition at higher potentials. However, the overpotential for which hydrogen and oxygen evolution occurs is strongly dependent on the pH and material involved. Khomenko et al. clearly demonstrated that MnO_2 and activated carbon displayed different voltage window stabilities in a neutral electrolyte.[31] When MnO_2 is polarized positively, potential values that are greater than the thermodynamic evolution of O_2 can be achieved because of the faradaic reactions at the electrode/electrolyte interface (Mn(IV) to Mn(III)). Furthermore, if activated carbon is negatively polarized in an aqueous electrolyte, high overpotential values for H_2 evolution can be achieved because hydrogen produced is adsorbed in the micropores of the carbon electrode.[31] Thus, when activated carbon is used as an anode and MnO_2 as a cathode, an extended voltage window can be achieved (up to 2 V).[31] Because energy density is proportional to the square of the voltage, increasing the voltage window quadratically increases the energy density.

It has further been shown that MnO_2 can achieve a theoretical specific capacitance of 1380 F g^{-1}, but this high capacitance has been limited to thin-film applications with ultra-low mass loadings.[30,32] In more practical applications, the typical capacitance of MnO_2 is on the order of 150−250 F g^{-1}.[33] The diminishing capacitance with scale is in part due to the low electrical conductivity exhibited by MnO_2 electrodes. Thus, composite carbon/MnO_2 electrodes have been explored as a method for achieving a conductive framework, while still utilizing fast faradaic reactions provided by the metal oxide.[34] Moreover, no pseudocapacitive metal oxide-carbon systems have ever been tested in a flowable electrode configuration.

In the present work, we examine the use of metal oxides as the active material in a flowable electrode. We chose to study manganese oxide as a model material for this application because it is a low cost, environmentally friendly, and abundant material. We report the electrochemical properties of a manganese oxide suspension-type electrode, and highlight the key aspects that are pivotal in the design of composite suspension electrodes for balanced rheological and electrochemical properties. Within this context, the role of the conductive additive concentration on conductivity and viscosity is studied and quantified. Furthermore, potentiodynamic electrochemical impedance spectroscopic methods are used to investigate and compare the charge storage mechanisms in suspension electrodes composed of manganese oxide and activated carbon. Finally, we demonstrate an expanded voltage window of ∼1.6 V in an asymmetric configuration when a manganese oxide suspension electrode is paired with an activated carbon suspension electrode.

2. EXPERIMENTAL SECTION

2.1. Materials. Potassium permanganate ($KMnO_4$) (≥ 99%), regent grade sulfuric acid (95-98 wt %), and pure ethanol (190 Proof) were purchased from Fisher Scientific and used in the synthesis of the manganese oxide. The active material in the carbon suspension was composed of YP-50F activated carbon (Kuraray Chemical Company, USA). Each suspension electrode studied employed a conductive additive, carbon black (100% compressed; Alfa Aesar, USA), and was studied in a neutral aqueous electrolyte (1 M Na_2SO_4) also purchased from Fisher Scientific.

2.2. Low-Temperature Hydrothermal Synthesis of MnO_2. Nanosized MnO_2 was prepared via a low-temperature hydrothermal route with slight modifications from a previous report.[33] Typically, 40 mL of deionized water was combined with 40 mL of ethanol, and then the pH was lowered to ∼2 by the addition of 1M sulfuric acid. In this solution, 0.45 g of $KMnO_4$ was dissolved under constant and rapid

dx.doi.org/10.1021/am501650q | ACS Appl. Mater. Interfaces 2014, 6, 8886−8893

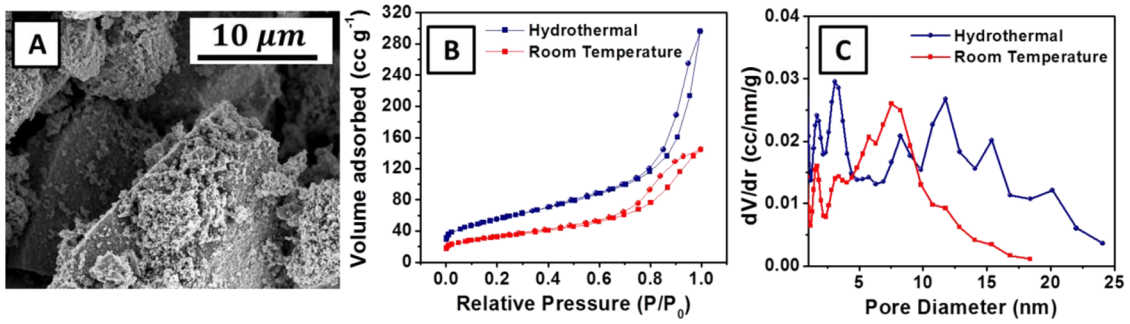

Figure 2. (A) SEM image of amorphous nano hydrothermal manganese oxide, (B) the nitrogen adsorption/desorption isotherms, and (C) the pore size distribution for the hydrothermal and room temperature synthesized manganese oxide.

stirring. After 2 min, the mixture was transferred to a Teflon-lined stainless steel autoclave and sealed and stored in an oven at 65 °C for 18 h. Afterward, the autoclave was naturally cooled to room temperature and the dark brown manganese oxide was washed extensively with deionized water and extracted by centrifugation. The sample was dried in air (24 h at 65°C) before use.

SEM images of the MnO_2 were obtained on Zeiss Supra 50VP (Carl Zeiss AG, Germany). Gas sorption at a relative pressure range from 0.05 to 0.30 P/P_0 was carried out in a Quadrasorb gas sorption instrument (Quantachrome, USA) with N_2 at −196 °C to determine the specific surface area (SSA) and pore size distribution. The average, volume-weighted pore size was derived from the cumulative pore volume by assuming slit-shaped pores and employing quenched-solid density functional theory (QSDFT) deconvolution of N_2-sorption isotherms.[35] Finally, X-ray diffraction was performed on a powder diffractometer (Siemens D500, Germany) using Cu Kα radiation (lB1.54 Å) with 0.02° 2θ steps and 1 s dwelling time.

Suspension Electrode Preparation and Electrochemical Characterization. The composite manganese oxide suspension electrodes were prepared by mixing the active material (manganese oxide) with a conductive additive (carbon black CB) and an electrolyte solution (1M Na_2SO_4). The solid:liquid ratio was kept constant at 20% by mass, where solid refers to the combined mass of MnO_2 and CB. Different ratios of MnO_2:CB (18:2, 16:4, and 14:6) were studied to examine the effects of conductivity, and connectivity (percolation) on the electrochemical performance of the composite MnO_2 suspension electrode (Figure 1Sb). The carbon based electrode was prepared as reported before.[36] Briefly, the active material (YP-50) was combined with CB with the gravimetric ratio of YP-50:CB was 8:1, and the solid:liquid ratio was 23% by mass.

The electrochemical performance of the suspension electrode was studied in a two-electrode static configuration, composed of two stainless steel current collectors (Figure 1Sa). The suspension electrodes were loaded into a channel designated by latex gaskets. The channel depth (electrode thickness) was 610 μm after compression (see the Supporting Information). A polyvinylidene fluoride (PVDF) membrane separator with a mesh width of 100 nm (Durapore; Merck Millipore, Germany) was used as the insulating separator between the two suspension electrodes.

Electrochemical measurements were performed at room temperature on a VMP3 potentiostat/galvanostat (BioLogic, France). Cyclic voltammetry (CV) was carried out at 2, 5, 10, 20, 50, and 100 mV s^{-1} sweep rates. From CV, the specific gravimetric capacitance (C_{sp}) was derived using the following equation.

$$C_{sp} = \frac{2}{\Delta U}\frac{\int i dV}{\nu m} \quad (1)$$

where ΔU is the width of the voltage window, i is the discharge current, V is the voltage, ν is the sweep rate, and m is the mass of carbon in one electrode. The factor of two accounts for the two electrode setup, assuming that the charge is evenly distributed between two capacitors in series.[37] In addition to two-electrode tests, in order to appropriately size the suspension electrodes in an asymmetric configuration (Figure 1b), the specific capacitance of each composite electrode based on MnO_2 and YP-50 was determined in a three-electrode set-up. In the three-electrode set-up, an oversized suspension electrode based on YP-50 was used as a counter electrode, a chlorided silver wire was used as the reference electrode, and working electrode was a volumetrically smaller suspension electrode made of either of MnO_2 or YP-50. The silver wire was chlorided by immersing it in bleach for ∼1 h and then rinsing with deionized water. The specific capacitance of the electrode was calculated using the equation

$$C = (\int i dV)/(\nu m V) \quad (2)$$

where m is the mass of the electroactive materials in the working electrode (g).

Each suspension electrode was tested with potentiodynamic electrochemical impedance spectroscopy (PEIS) to understand how composition, and arrangement (symmetric/asymmetric) affected electrode kinetics and conductivity. The ohmic resistance of the static cell, R_Ω, was determined from the impedance spectrum intersection with the real axis and was compared for each composite suspension electrode studied. Furthermore, PEIS was used to evaluate the active material utilization by plotting the real part of the impedance plot against the $\omega^{-1/2}$, where ω is the frequency. All spectra were run in the frequency range of 200 kHz to 10 mHz at a sine wave signal amplitude of 10 mV.

2.3. Rheology. The viscosity of the MnO_2 composite suspension electrode with a MnO_2:CB ratio of 16:4 (20% solid:liquid) and the 23 wt % YP-50 suspension electrode was characterized through rheological studies. For these studies, an AR 2000 rheometer (TA Instruments, USA) was used at room temperature at shear rates ranging from 1 s^{-1} to 200 s^{-1}. The suspension (∼25 mL) was tested with a concentric cylinders geometry set-up (see the Supporting Information).

3. RESULTS AND DISCUSSION

3.1. Hydrothermal Synthesis. A facile and low-energy (low-temperature) process was used for the synthesis of MnO_2.

As a strong oxidizer $KMnO_4$ readily reduces to MnO_2 in the presence of ethanol (reductant). The possible mechanism for this oxidation/reduction reaction can be described by eq 3[33,38]:

$$CH_3CH_2OH + MnO_4^- \rightarrow CH_3COO^- + H_2O + MnO_2 \quad (3)$$

X-ray diffraction was performed on the sample, but no distinguishable peaks were visible indicating that the sample lacked any crystalline structure and was amorphous by nature. Figure 2a is a typical SEM of the hydrothermally prepared MnO_2. The structure consists of MnO_2 nanoparticles that have formed micrometer size agglomerates.

Figure 2b shows the adsorption-desorption isotherm for a sample of MnO_2 obtained through simple precipitation at room temperature and the low-temperature hydrothermally precipi-

tated sample. Both samples demonstrate type IV hysteresis loops at relative pressure between 0 and 1.0, which is characteristic of a mesoporous structure. When employing a density functional theory (DFT) model with the adsorption data, it was determined that the hydrothermal MnO_2 had a specific surface area (SSA) of 192 m^2 g^{-1} whereas the room temperature precipitated MnO_2 had a SSA of 115 m^2 g^{-1}. While capacitance is not directly related to surface area, because of the possible existence of charge storage in the bulk, it has been shown in some cases to increase the capacitance of the electrode by allowing for greater chemisorption of the working cation.[39] From the Barrett–Joyner–Halenda (BJH) pore size distribution in Fig. 2c it is clear that the hydrothermal process creates a bi-modal distribution of micro and mesopores, which can explains the observed increase in surface area. Both samples are mesoporous in nature; however, it appears that the hydrothermal reaction expands the mesopores which in some cases leads to the formation of micropores, or a broad distribution of mesopores.

3.2. Composite Percolating Manganese Oxide Suspension Electrode. The role of charge percolation and active material connectivity in a suspension electrode composed of MnO_2 was examined by altering the ratio of active material to conductive additive (see the Supporting Information). Carbon black (a conductive additive) serves two primary roles in electrodes: (1) it increases the overall electrode conductivity for efficient electron transport and (2) and provides bridges (connection points) between active materials forming percolation networks (Figure 1Sb). Both properties enhance the charge and ion transport (rate performance) properties of the suspension electrode, which is otherwise inherently diffusion limited because of the thicker more tortuous pathways in suspension electrodes.[40] Thus, while film electrodes typically contain 5 wt % CB, in order to balance trade-offs between energy and power densities, suspension electrodes typically use 11 wt % CB to achieve a percolation network suitable for a range of rates.[12,36] Nevertheless, it should be noted that in suspension electrodes the low density nature of carbon black (~0.15 g/mL) yields a third effect, an increase in viscosity (increase in active material connectivity). Furthermore, because of CB's low specific surface area (~75 m^2 g^{-1}), it negatively affects the capacitance (ion adsorption capacity) and energy density of a system. Thus, there are numerous factors to consider in the design of percolating networks of MnO_2.[41,42]

Figure 3 demonstrates the effects of CB composition (2/4/6%) on the electrochemical performance of the MnO_2 suspension electrode in a two-electrode symmetric configuration. The rate performance of three suspension electrodes based on 20% solid material (MnO_2+CB) is shown in Figure 3a. Almost across all rates studied, 4% CB:16% MnO_2 displayed the greatest capacitance, whereas the composite electrode with the greatest proportion of MnO_2 shows the lowest capacitance. At the highest sweep rate (100 mV s^{-1}) the suspension with the greatest proportion of CB (6%) exhibited the greatest capacitance. This can be attributed to better conductivity across the electrode. Thus, a composite electrode with a carbon support for conductivity is necessary for suspension electrodes in order to achieve a high utilization of MnO_2 pseudocapacity. It was observed that the addition of CB not only affected the conductivity of the suspension electrode but also the viscosity, as will be discussed later. Increasing the viscosity leads to better connectivity between the active materials which enables better transport of charge across the electrode, which affects the

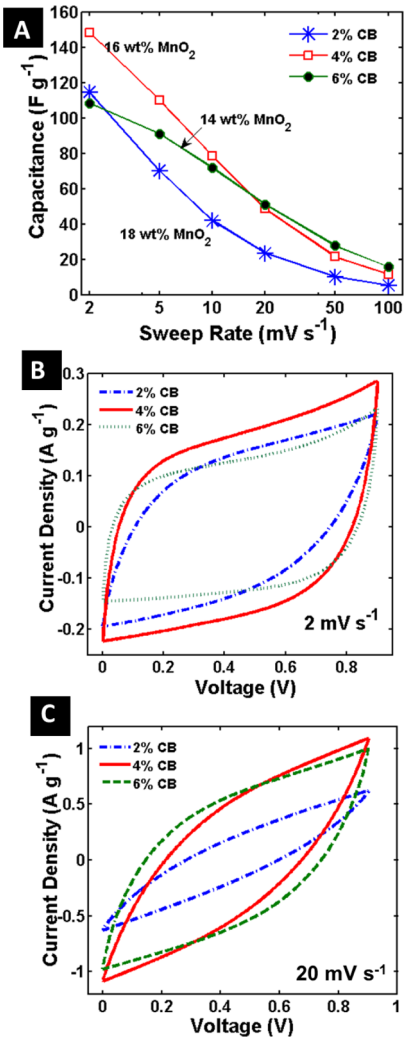

Figure 3. (A) Rate performance of symmetric manganese oxide suspension based on different ratios of carbon black (2, 4, and 6 wt %). Typical cyclic voltammograms at (B) a low sweep rate 2 mV s^{-1} and (C) at a higher rate 20 mV s^{-1}.

overall performance of the suspension electrode. We attribute the poor rate performance and low capacitance of the 18 wt % MnO_2 suspension electrode to its lower conductivity and lower connectivity between particles of active materials.

Figure 3b shows a characteristic cyclic voltammagram for various MnO_2 suspension electrodes with different amounts of CB at a low sweep rate of 2 mV s^{-1}. The electrodes with 4 and 6% CB demonstrated less resistive curves than the electrode with 2% CB, which is apparent because the curves are more rectangular. The addition of CB makes the composite electrode more conductive, which leads to better transport pathways between active materials. The CVs of the MnO_2 composite suspension electrode as an active material will not resemble traditional capacitive materials (i.e., activated carbon) because the charge storage mechanism is more pseudocapacitive in nature and involves the intercalation of alkali metal cations (Na^+) (bulk faradaic reactions) and surface faradaic reaction.[25,29,30] Thus, the cyclic voltammograms of the symmetric MnO_2 composite are not perfectly rectangular for any combination of active material/conductive additive.

At a higher rate of 20 mV s^{-1}, we observe all the curves becoming much more resistive (Figure 3c). The area under the

dx.doi.org/10.1021/am501650q | ACS Appl. Mater. Interfaces 2014, 6, 8886–8893

curve is proportional to the capacitance, and thus it is apparent that the composite MnO_2 electrode with 6% CB demonstrates the greatest capacitance. This demonstrates the fact that at high scan rates, charge percolation becomes a dominating factor in suspension electrodes, and thus suspension electrodes benefit from a greater composition of carbon black. There are numerous trade-offs in terms of material utilization, rate performance, and conductivity that need to be considered in the design of composite suspension electrodes composed of metal oxides. In the composite electrode with the greatest proportion of MnO_2 we observe low utilization because of poor conductivity and connectivity. To balance these factors, and based on the assumption that suspension electrode will most likely be used for rates below 20 mV s^{-1}, in this study the optimal composite electrode was determined to be the composition with 4% CB/16% MnO_2. For the foregoing analysis, we will refer to this suspension electrode as CB4:$MnO_2$16.

3.3. Rheological Performance of Suspension Electrodes. The suspension electrodes studied were characterized for their rheological behavior and the results are shown in Figure S2 in the Supporting Information. As previously reported, suspension electrodes demonstrate shear-thinning (pseudoplastic) behavior as the apparent viscosity decreases with shear rate.[36] Thus, the dynamics were modeled with the Ostwald-de Waele power law model approximated by eq 4.

$$\eta = k\gamma^{n-1} \tag{4}$$

where η is the viscosity, k is the consistency index, γ is the shear rate, and n is the shear thinning index (see Table S1 in the Supporting Information). Generally, as k increases (the curve moves upward) and the system becomes more viscous. The CB4:$MnO_2$16 (20 wt %) suspension electrode demonstrated the greatest consistency index of 14.01. The corresponding 20 wt % AC-based suspension electrode demonstrated significantly less viscous effects with a consistency index of ~12.08. Nevertheless, the two suspension electrodes had similar viscosities. The increase in viscosity is in part due to the required higher ratio of conductive additive (CB) in the suspension electrode.

Increasing the wt % of active material has been shown to be advantageous for electrochemical properties.[36] Thus, since the activated carbon electrode had a lower viscosity at 20 wt %, we chose to examine a 23 wt % AC-based electrodes, as it has been previously studied and optimized.[36] Thus, the increase in weight percentage would enable the electrodes to have similar rheological performances. For the forgoing asymmetric set-up, we use an AC suspension electrode (21% AC:2.5% CB:76.5% Na_2SO_4) and the MnO_2 suspension (CB4:$MnO_2$16).

3.4. Activated Carbon and MnO_2 Suspension Electrode Comparison. The AC (CB2.5:AC20) and MnO_2 (CB4:$MnO_2$16) suspension electrodes were studied in a symmetric two electrode set-up in order to quantify the electrochemical and kinetic properties of the different suspension systems. Figure 4a shows the Nyquist plots for each composite suspension electrode. The x-axis intercept in the high frequency region is the equivalent series resistance (ESR). The AC suspension (~1 Ω) demonstrates a slightly lower ESR than the MnO_2 suspension (~1.5 Ω). We attribute this difference to the lower conductivity exhibited in MnO_2 in comparison to activated carbon. The vertical line apparent in the low frequency region for the AC suspension electrode is characteristic of purely capacitive behavior. In contrast, the

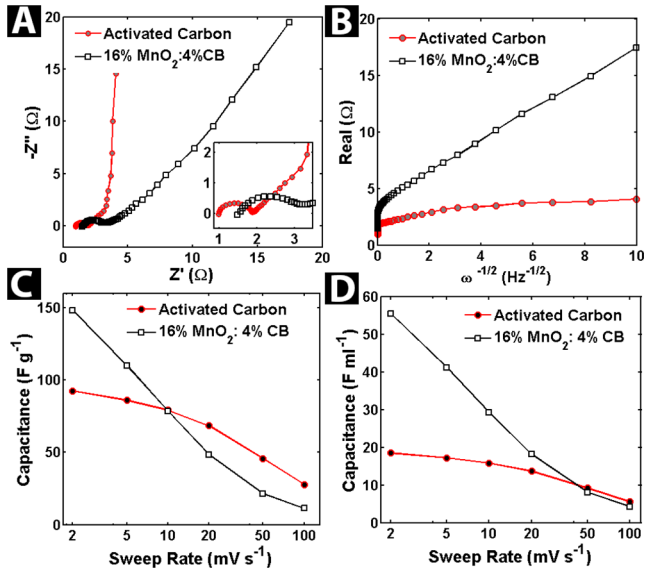

Figure 4. (A) Nyquist plots of activated carbon suspension and optimized manganese oxide suspension (16% MnO_2:4% CB:80% 1 M Na_2SO_4) in the frequency of 200 kHz to 10 mHz and (B) the relationship between the real Z_{re} and $\omega^{-1/2}$ at low frequencies. The rate performance of the optimized activated carbon and manganese oxide suspension electrodes in terms of (C) gravimetric and (D) volumetric capacitance.

MnO_2 suspension electrode's low frequency region is characterized by a 45° angle, which is characteristic of a diffusion limited process. The impedance associated with this low frequency diffusion processes is the Warburg impedance[43] and can be represented by eq 5

$$Z_w = [\sigma\omega^{-1/2} - j(\sigma\omega^{-1/2})] = \omega^{-1/2}\sigma[1 - j] \tag{5}$$

where Z_w is the Warburg impedance, σ is the Warburg coefficient, ω is the frequency, and j is an imaginary number. In Figure 4b, when we plot the real part of the Nyquist plot as a function of the inverse square root of the frequency, we observe the Warburg coefficient (slope) is greater for the MnO_2 electrode than the activated carbon electrode. The small slope demonstrated by the AC suspension electrode is characteristic of high diffusion rates and high utilization of the active material. The MnO_2 composite suspension electrode has a greater slope, indicative of a pseudocapacitive behavior and a more complex charge transfer processes.

The low-frequency region of the Nyquist plot is indictive of semi-infinite diffusion and finite diffusion dynamics. The semi-inifinite diffusion region is characterized by a slope of 45°, whereas infinite diffusion occurs when the line become vertical. The vertex between these regions ("knee frequency") represents the maximum frequency for which capacitive behavior dominates. Thus, for high power applications, it is ideal to have high knee frequencies. In the suspension electrode based on activated carbon, the knee frequency occurs at ~104 mHz. On the other hand, the suspension based on MnO_2 does not exhibit a knee frequency, which suggests that there is not much charge storage within the diffusion limited bulk region,[32,44] and thus in our suspension system we may be limited to surface reactions presented in Figure 1a, and thus the accessible surface area is an important consideration.

Panels c and d in Figure 4 show the rate performance of the different suspension electrodes gravimetrically and volumetri-

dx.doi.org/10.1021/am501650q | ACS Appl. Mater. Interfaces 2014, 6, 8886−8893

cally normalized. At low sweep rates, the capacitance of MnO_2 (149 F g^{-1} at 2 mV s^{-1}) exceeds AC (93 F g^{-1} at 2 mV s^{-1});however, because of poor conductivity, the gravimetric rate performance of MnO_2 drops quickly with sweep rate. Nevertheless, for a flowable system, the volumetric capacitance is important to consider. The density of the activated carbon is ~0.20 g/mL, whereas the density of the synthesized MnO_2 is ~0.37 g/mL. When the densities of the active materials are considered, the capacitance of the MnO_2 (55 F mL^{-1} at 2 mV s^{-1}) far exceeds that of the AC (18.5 F mL^{-1} at 2 mV s^{-1}), even at high rates.

3.5. Asymmetric MnO_2/Activated Carbon Suspension Electrode. Figure 5 shows comparative cyclic voltammograms

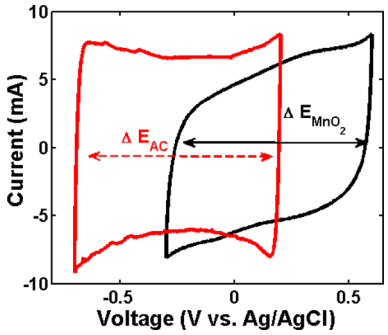

Figure 5. Cyclic voltammetry in a three-electrode configuration for the activated carbon based suspension electrode (21% AC:2.5% CB:76.5% Na_2SO_4) and the manganese-oxide composite electrode (16% MnO_2:4% CB:80% 1 M Na_2SO_4) at 5 mV s^{-1}. The different materials occupy different voltage stability windows when based in neutral 1 M sodium sulfate electrolyte.

for the manganese-based suspension (CB4:$MnO_2$16) and the activated-carbon based suspension (20% AC: 3%CB) in a three-electrode configuration. The two materials occupy different voltage stability windows when assessed in a neutral electrolyte (1M Na_2SO_4). Thus, by using an asymmetric configuration with an activated carbon suspension as the anode, and manganese oxide suspension as the cathode, an expanded voltage window of ~1.4−1.6 V can be achieved. The specific capacitance derived from the three-electrode tests at 5 mV s^{-1} is ~133 F/g (49 F/ml) for the manganese oxide composite suspension electrode and ~134 F/g (27 F/ml) for the suspension based on activated carbon. In order to achieve an expanded voltage window the charges at each electrode must be balanced. In this study we sized our anode and cathode according to the mass balance method[31,45]

$$R = \frac{m_+}{m_-} = \frac{C_-\Delta E_-}{C_+\Delta E_+} \approx 2 \quad (6)$$

where m_+ and m_- are the mass of the active material, C_+ and C_- are the specific capacitance, and ΔE_+ and ΔE_- are the voltage windows for the specific capacitance of the positive and negative electrodes, respectively.

Figure 6a exhibits the expanded voltage window that can be achieved with the optimized asymmetric configuration (anode, 21% AC:2.5% CB:76.5% 1 M Na_2SO_4 and cathode: CB4:$MnO_2$16). Up to 1.75 V, the curves demonstrate a linear charge and discharge curve with similar slopes indicating good reversibility. Furthermore, in Figure 6b the coulombic efficiency decreases only slightly between 1 and 1.5 V, and the device still maintains good coulombic efficiency (~96%) up to a voltage window of 1.75 V. The expansion of the voltage window inherently enhances the energy density, but we also see that through the expansion of the voltage window we get an approximate increase of 17% in the cell capacitance (Figure 6b). For the galvanostatic cycling data we calculated the capacitance normalized to the mass of the active material in both electrodes with eq 7.

$$C = \frac{Idt}{mdV} \quad (7)$$

On the basis of the previous voltage window expansion, we fully characterized the asymmetric configuration in a voltage window of 1.6 V. In an asymmetric configuration, we observed the cyclic voltammograms demonstrated a more ideally polarizable behavior (rectangular) in Figure 7a. Furthermore, the rate performance is greatly improved over the symmetric two-electrode set-up comprised on MnO_2 suspension electrodes (Figure 7b). However, at low rates the capacitance is similar to the symmetric MnO_2 suspension electrode system, but demonstrates an expanded voltage window of ~1.6 V.

The Nyquist plot of the asymmetric device is shown in Figure 7c and demonstrates a very low ESR value of ~0.5 Ω compared to the symmetric cells studied before. We attribute this to the fact that the asymmetric device had a smaller weight and volume than our original devices because of the mass balancing thus reducing the diffusion pathways. Nevertheless, in the low frequency region, the plot looks more similar to the plot of the AC suspension electrode with a nearly vertical line indicating better utilization of the material.

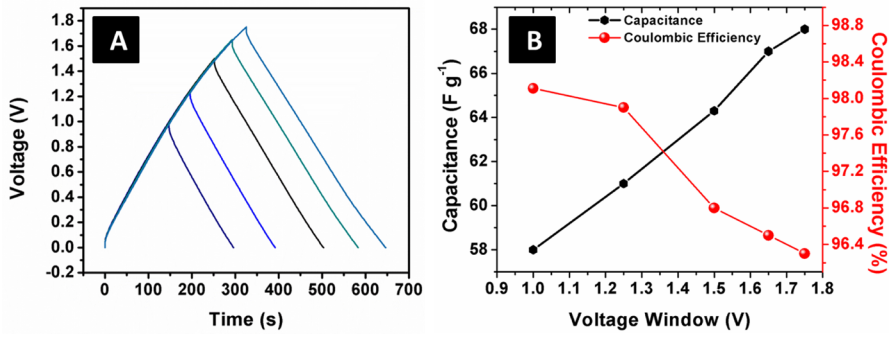

Figure 6. (A) Expansion of voltage window exhibited by galvanostatic charge/discharge at 200 mA g^{-1} and (B) capacitance and coulombic efficiencies at different voltage ranges.

dx.doi.org/10.1021/am501650q | ACS Appl. Mater. Interfaces 2014, 6, 8886−8893

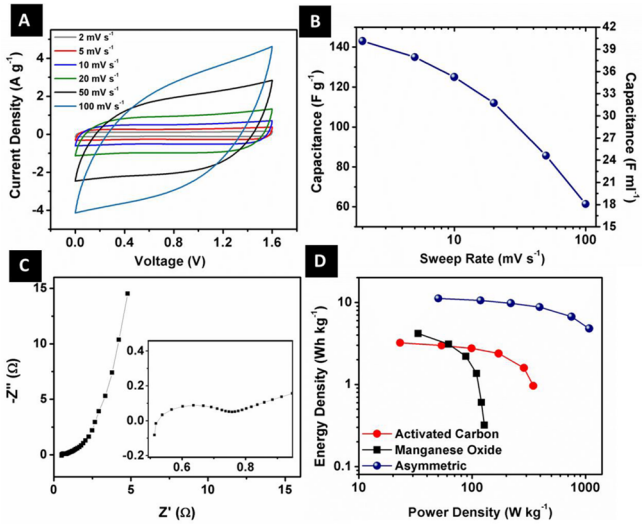

Figure 7. Cyclic voltammagram of asymmetric devices with a mass ratio of $R = 2$ over the range of (A) 2−100 mV s^{-1} and (B) rate performance. (C) Potentiostatic electrochemical impedance spectroscopy of asymmetric device and (D) Ragone plot of symmetric systems composed of manganese oxide, activated carbon, and asymmetric device.

The overall benefit of an expanded voltage window can be observed when comparing the energy and power densities of the device. The average power density and energy densities were calculated across all rates studied with eqs 8 and 9

$$p_{ave} = \frac{E}{t} \tag{8}$$

$$E = \frac{1}{2}CV^2 \tag{9}$$

where t is the discharge time, and C is the specific capacitance, and V is the voltage window. A Ragone plot of the asymmetric and symmetric suspension devices is shown in Figure 7d. The MnO_2 symmetric suspension electrode shows a sharp decline in energy density with increasing power density, while the symmetric device based on activated carbon shows a slower response. Furthermore, the power and energy densities of the symmetric MnO_2 device is only slightly greater in term of energy and power density than the symmetric AC device. However, the asymmetric devices far exceed the symmetric devices reaching an energy density of 11 Wh kg^{-1} at a power density of 50 W kg^{-1}. These values are similar to reported values on film electrodes. Thus, with further material optimization, an asymmetric electrochemical flow capacitor may be an avenue for achieving high energy and power densities while utilizing low-cost and abundant materials based on a neutral electrolyte system. Introduction of redox materials can potentially make flow capacitors competitive with flow batteries in terms of energy density.

4. CONCLUSIONS

The electrochemical performance of a composite flowable suspension-type electrode based on MnO_2 has been studied in a two-electrode device. It was shown that a balanced approach, considering the material capacitance, rate performance, and rheological properties is important for the design of these electrochemical systems. The rate performance of manganese-oxide suspension electrodes can be enhanced by the addition of conductive additives such as carbon black, but at the cost of viscosity. Furthermore, the amorphous manganese oxide in the suspension form utilized here, demonstrated mainly surface charge storage reactions. Increasing accessible surface area or forming crystalline MnO_2 structures may yield improved capacitance. An expanded voltage window of 1.6 V can be achieved in a charge-balanced asymmetric device with an activated carbon suspension as the anode, and a composite manganese oxide suspension electrode as the cathode. This leads to a substantial increase in the energy and power densities of a suspension electrode system based in a neutral electrolyte. This work demonstrates a cost-effective, pragmatic, and scalable approach toward obtaining high energy and power densities by a flowable electrode systems for grid scale energy storage

■ ASSOCIATED CONTENT

Ⓢ Supporting Information

Background information regarding experimental procedure, percolation networks in suspension electrodes, and relevant rheological information in included. This material is available free of charge via the Internet at http://pubs.acs.org.

■ AUTHOR INFORMATION

Corresponding Authors

*E-mail: yg36@drexel.edu.
*E-mail: eck32@drexel.edu.

Notes

The authors declare no competing financial interest.

■ ACKNOWLEDGMENTS

The authors acknowledge the support from Fluid Interface Reactions, Structures and Transport (FIRST) Center, an Energy Frontier Research Center funded by the U.S. Department of Energy, Office of Science, Office of Basic Energy Sciences, and Ben Franklin Technology Partners of Southeastern Pennsylvania Energy Commercialization Institute (Grant 001389-002). K.B.H. was supported by the NSF Graduate Research Fellowship (Grant 1002809).

■ REFERENCES

(1) Whitacre, J.; Wiley, T.; Shanbhag, S.; Wenzhuo, Y.; Mohamed, A.; Chun, S.; Weber, E.; Blackwood, D.; Lynch-Bell, E.; Gulakowski, J. An Aqueous Electrolyte, Sodium Ion Functional, Large Format Energy Storage Device for Stationary Applications. *J. Power Sources* **2012**, *213*, 255−264.

(2) Yang, Z.; Zhang, J.; Kintner-Meyer, M. C.; Lu, X.; Choi, D.; Lemmon, J. P.; Liu, J. Electrochemical Energy Storage for a Green Grid. *Chem. Rev.* **2011**, *111*, 3577.

(3) Dunn, B.; Kamath, H.; Tarascon, J.-M. Electrical Energy Storage for the Grid: A Battery of Choices. *Science* **2011**, *334*, 928−935.

(4) Hittinger, E.; Whitacre, J.; Apt, J. What Properties of Grid Energy Storage are Most Valuable? *J. Power Sources* **2012**, *206*, 436−449.

(5) Whitacre, J.; Tevar, A.; Sharma, S. $Na_4Mn_9O_{18}$ as a Positive Electrode Material for an Aqueous Electrolyte Sodium-Ion Energy Storage Device. *Electrochem. Commun.* **2010**, *12*, 463−466.

(6) Gu, S.; Gong, K.; Yan, E. Z.; Yan, Y. A Multiple Ion-Exchange Membrane Design for Redox Flow Batteries. *Energy Environ. Sci.* **2014**, DOI: 10.1039/c4ee00165f.

(7) Skyllas-Kazacos, M.; Chakrabarti, M.; Hajimolana, S.; Mjalli, F.; Saleem, M. Progress in Flow Battery Research and Development. *J. Electrochem. Soc.* **2011**, *158*, R55−R79.

(8) Skyllas-Kazacos, M.; Rychcik, M.; Robins, R. G.; Fane, A.; Green, M. New All-Vanadium Redox Flow Cell. *J. Electrochem. Soc.* **1986**, *133*, 1057−1058.

(9) Huskinson, B.; Marshak, M. P.; Suh, C.; Er, S.; Gerhardt, M. R.; Galvin, C. J.; Chen, X.; Aspuru-Guzik, A.; Gordon, R. G.; Aziz, M. J.; Metal-Free Organic-Inorganic, A. Aqueous Flow Battery. *Nature* **2014**, *505*, 195−198.
(10) Duduta, M.; Ho, B.; Wood, V. C.; Limthongkul, P.; Brunini, V. E.; Carter, W. C.; Chiang, Y.-M. Semi-Solid Lithium Rechargeable Flow Battery. *Adv. Energy Mater.* **2011**, *1*, 511−516.
(11) Presser, V.; Dennison, C. R.; Campos, J.; Knehr, K. W.; Kumbur, E. C.; Gogotsi, Y. Electrochemical Flow Cells: The Electrochemical Flow Capacitor: A New Concept for Rapid Energy Storage and Recovery. *Adv. Energy Mater.* **2012**, *2*, 911−911.
(12) Hatzell, K. B.; Beidaghi, M.; Campos, J. W.; Dennison, C. R.; Kumbur, E. C.; Gogotsi, Y.; High, A. A High Performance Pseudocapacitive Suspension Electrode for the Electrochemical Flow Capacitor. *Electrochim. Acta* **2013**, *111*, 888−897.
(13) Youssry, M.; Madec, L.; Soudan, P.; Cerbelaud, M.; Guyomard, D.; Lestriez, B. Nonaqueous Carbon Black Suspensions for Lithium-Based Redox Flow Batteries: Rheology and Simultaneous Rheo-Electrical Behavior. *Phys. Chem. Chem. Phys.* **2013**, *15*, 14476−14486.
(14) Fan, F.; Woodford, W.; Li, Z.; Baram, N.; Smith, K. C.; Helal, A.; McKinley, G. H.; Carter, W. C.; Chiang, Y.-M. Polysulfide Flow Batteries Enabled by Percolating Nanoscale Conductor Networks. *Nano Lett.* **2014**, *14*, 2210−2218.
(15) Jeon, S.-I.; Park, H.-R.; Yeo, J.-G.; Yang, S.; Cho, C. H.; Han, M. H.; Kim, D.-K. Desalination via a New Membrane Capacitive Deionization Process Utilizing Flow Electrodes. *Energy Environ. Sci.* **2013**, *6*, 1471−1475.
(16) Hatzell, K. B.; Iwama, E.; Ferris, A.; Daffos, B.; Urita, K.; Tzedakis, T.; Chauvet, F.; Taberna, P.-L.; Gogotsi, Y.; Simon, P. Capacitive Deionization Concept Based on Suspension Electrodes without Ion Exchange Membranes. *Electrochem. Commun.* **2014**, *43*, 18−21.
(17) Jeon, S. I.; Park, J.-S.; Yeo, J.-G.; Yang, S.; Choi, J.; Kim, D. K. Ion Storage and Energy Recovery of Flow-Electrode Capacitive Deionization Process. *J. Mater. Chem. A* **2014**, *2*, 6378−6383.
(18) Simon, P.; Gogotsi, Y. Materials for Electrochemical Capacitors. *Nat. Mater.* **2008**, *7*, 845−854.
(19) Roldán, S.; Blanco, C.; Granda, M.; Menéndez, R.; Santamaría, R. Towards a Further Generation of High Energy Carbon Based Capacitors by Using Redox-Active Electrolytes. *Angew. Chem., Int. Ed.* **2011**, *50*, 1699−1701.
(20) Mai, L.-Q.; Minhas-Khan, A.; Tian, X.; Hercule, K. M.; Zhao, Y.-L.; Lin, X.; Xu, X., Synergistic Interaction between Redox-Active Electrolyte and Binder-Free Functionalized Carbon for Ultrahigh Supercapacitor Performance. *Nat. Commun.* **2013**, *4*, DOI:10.1038/ncomms3923.
(21) Conway, B. *Electrochemical Supercapacitors: Scientific Fundamentals and Technological Applications*; Kluwer Academic/Plenum: New York, 1999.
(22) Conway, B.; Birss, V.; Wojtowicz, J. The Role and Utilization of Pseudocapacitance for Energy Storage by Supercapacitors. *J. Power Sources* **1997**, *66*, 1−14.
(23) Conway, B. E. Transition from "Supercapacitor" to "Battery" Behavior in Electrochemical Energy Storage. *J. Electrochem. Soc.* **1991**, *138*, 1539−1548.
(24) Lang, X.; Hirata, A.; Fujita, T.; Chen, M. Nanoporous Metal/Oxide Hybrid Electrodes for Electrochemical Supercapacitors. *Nat. Nanotechnol.* **2011**, *6*, 232−236.
(25) Wei, W.; Cui, X.; Chen, W.; Ivey, D. G. Manganese Oxide-Based Materials as Electrochemical Supercapacitor Electrodes. *Chem. Soc. Rev.* **2011**, *40*, 1697−1721.
(26) Wang, G.; Zhang, L.; Zhang, J. A Review of Electrode Materials for Electrochemical Supercapacitors. *Chem. Soc. Rev.* **2012**, *41*, 797−828.
(27) Zhao, Y.; Si, S.; Wang, L.; Liao, C.; Tang, P.; Cao, H. Electrochemical Study on Polypyrrole Microparticle Suspension as Flowing Anode for Manganese Dioxide Rechargeable Flow Battery. *J. Power Sources* **2014**, *248*, 962−968.
(28) Zhao, Y.; Si, S.; Wang, L.; Tang, P.; Cao, H. Electrochemical Behavior of Polyaniline Microparticle Suspension as Flowing Anode for Rechargeable Lead Dioxide Flow Battery. *J. Electrochem. Soc.* **2014**, *161*, A330−A335.
(29) Lee, H. Y.; Goodenough, J. B. Supercapacitor Behavior with KCl Electrolyte. *J. Solid State Chem.* **1999**, *144*, 220−223.
(30) Toupin, M.; Brousse, T.; Bélanger, D. Charge Storage Mechanism of MnO2 Electrode Used in Aqueous Electrochemical Capacitor. *Chem. Mater.* **2004**, *16*, 3184−3190.
(31) Khomenko, V.; Raymundo-Pinero, E.; Beguin, F. Optimisation of an Asymmetric Manganese Oxide/Activated Carbon Capacitor Working at 2V in Aqueous Medium. *J. Power Sources* **2006**, *153*, 183−190.
(32) Pang, S. C.; Anderson, M. A.; Chapman, T. W. Novel Electrode Materials for Thin-Film Ultracapacitors: Comparison of Electrochemical Properties of Sol-Gel-Derived and Electrodeposited Manganese Dioxide. *J. Electrochem. Soc.* **2000**, *147*, 444−450.
(33) Liu, J.-L.; Fan, L.-Z.; Qu, X. Low Temperature Hydrothermal Synthesis of Nano-Sized Manganese Oxide for Supercapacitors. *Electrochim. Acta* **2012**, *66*, 302−305.
(34) Raymundo-Pinero, E.; Khomenko, V.; Frackowiak, E.; Beguin, F. Performance of Manganese Oxide/CNTs Composites as Electrode Materials for Electrochemical Capacitors. *J. Electrochem. Soc.* **2005**, *152*, A229−A235.
(35) Gor, G. Y.; Thommes, M.; Cychosz, K. A.; Neimark, A. V. Quenched Solid Density Functional Theory Method for Characterization of Mesoporous Carbons by Nitrogen Adsorption. *Carbon* **2012**, *50*, 1583−1590.
(36) Campos, J.; Beidaghi, M.; Hatzell, K. B.; Dennison, C.; Presser, V.; Kumbur, E. C.; Gogotsi, Y. Investigation of Carbon Materials for Use as a Flowable Electrode in Electrochemical Flow Capacitors. *Electrochim. Acta* **2013**, *98*, 123−130.
(37) Stoller, M. D.; Ruoff, R. S. Best Practice Methods for Determining an Electrode Material's Performance for Ultracapacitors. *Energy Environ. Sci.* **2010**, *3*, 1294−1301.
(38) Subramanian, V.; Zhu, H.; Wei, B. Alcohol-Assisted Room Temperature Synthesis of Different Nanostructured Manganese Oxides and their Pseudocapacitance Properties in Neutral Electrolyte. *Chem. Phys. Lett.* **2008**, *453*, 242−249.
(39) Tang, X.; Liu, Z.-h.; Zhang, C.; Yang, Z.; Wang, Z. Synthesis and Capacitive Property of Hierarchical Hollow Manganese Oxide Nanospheres with Large Specific Surface Area. *J. Power Sources* **2009**, *193*, 939−943.
(40) Ebner, M.; Chung, D. W.; García, R. E.; Wood, V., Tortuosity Anisotropy in Lithium-Ion Battery Electrodes. *Adv. Energy Mater.* **2013**, *4*, DOI: 10.1002/aenm.201301278.
(41) Jiang, J.; Kucernak, A. Electrochemical Supercapacitor Material Based on Manganese Oxide: Preparation and Characterization. *Electrochim. Acta* **2002**, *47*, 2381−2386.
(42) Dennison, C.; Beidaghi, M.; Hatzell, K.; Campos, J.; Gogotsi, Y.; Kumbur, E. Effects of Flow Cell Design on Charge Percolation and Storage in the Carbon Slurry Electrodes of Electrochemical Flow Capacitors. *J. Power Sources* **2014**, *247*, 489−496.
(43) Bard, A. J.; Faulkner, L. R. *Electrochemical Methods: Fundamentals and Applications*; Wiley: New York, 1980; *Vol. 2*.
(44) Yoon, S.-B.; Jegal, J.-P.; Roh, K. C.; Kim, K.-B. Electrochemical Impedance Spectroscopic Investigation of Sodium Ion Diffusion in MnO2 Using a Constant Phase Element Active in Desired Frequency Ranges. *J. Electrochem. Soc.* **2014**, *161*, H207−H213.
(45) Brousse, T.; Taberna, P.-L.; Crosnier, O.; Dugas, R.; Guillemet, P.; Scudeller, Y.; Zhou, Y.; Favier, F.; Bélanger, D.; Simon, P. Long-term Cycling Behavior of Asymmetric Activated Carbon/MnO_2 Aqueous Electrochemical Supercapacitor. *J. Power Sources* **2007**, *173*, 633−641.